



HAL
open science

A physically based method for soil evaporation estimation by revisiting the soil drying process

Yunquan Wang, Olivier Merlin, Gaofeng Zhu, Kun Zhang

► **To cite this version:**

Yunquan Wang, Olivier Merlin, Gaofeng Zhu, Kun Zhang. A physically based method for soil evaporation estimation by revisiting the soil drying process. *Water Resources Research*, 2019, 55 (11), pp.9092-9110. 10.1029/2019WR025003 . hal-02384848

HAL Id: hal-02384848

<https://hal.science/hal-02384848>

Submitted on 15 Dec 2020

HAL is a multi-disciplinary open access archive for the deposit and dissemination of scientific research documents, whether they are published or not. The documents may come from teaching and research institutions in France or abroad, or from public or private research centers.

L'archive ouverte pluridisciplinaire **HAL**, est destinée au dépôt et à la diffusion de documents scientifiques de niveau recherche, publiés ou non, émanant des établissements d'enseignement et de recherche français ou étrangers, des laboratoires publics ou privés.

A physically based method for soil evaporation estimation by revisiting the soil drying process

Yunquan Wang^{1, 2*}, Oliver Merlin³, Gaofeng Zhu⁴, Kun Zhang⁵

¹ School of Environmental Studies, China University of Geosciences at Wuhan, 430074, PR China,

² Laboratory of Basin Hydrology and Wetland Eco-restoration, China University of Geosciences, Wuhan 430074, PR China,

³ CESBIO, Université de Toulouse, CNES, CNRS, IRD, UPS, Toulouse, France,

⁴ Key Laboratory of Western China's Environmental Systems (Ministry of Education), Lanzhou University, Lanzhou 730000, China,

⁵ Institute of Tibetan Plateau Research, Chinese Academy of Sciences, Beijing 100084, China.

*Corresponding Author: Yunquan Wang, School of Environmental Studies, China University of Geosciences at Wuhan, Lumo Rd.388, Hongshan District, Wuhan, China, 430074 (wangyq@cug.edu.cn)

Abstract

While numerous models exist for soil evaporation estimation, they are more or less empirically based either in the model structure or in the determination of introduced parameters. The main difficulty lies in representing the water stress factor, which is usually thought to be limited by capillarity-supported water supply or by vapor diffusion flux. Recent progress in understanding soil hydraulic properties, however, have found that the film flow, which is often neglected, is the dominant process under low moisture conditions. By including the impact of film flow, a reexamination on the typical evaporation process found that this usually neglected film flow might be the dominant process for supporting the stage- II evaporation (i.e. the fast falling rate stage), besides the generally accepted capillary-flow-supported stage- I evaporation and the vapor-diffusion-controlled stage- III evaporation. A physically based model for

27 estimating the evaporation rate was then developed by parameterizing the
28 Buckingham-Darcy's law. Interestingly, the empirical Bucket model was found to be a
29 specific form of the proposed model. The proposed model requires the in-equilibrium
30 relative humidity as the sole input for representing water stress and introduces no
31 adjustable parameter in relation to soil texture. The impact of vapor diffusion was also
32 discussed. Model testing with laboratory data yielded an excellent agreement with
33 observations for both thin soil and thick soil column evaporation experiments. Model
34 evaluation at 15 field sites generally showed a close agreement with observations,
35 with a great improvement in the lower range of evaporation rates in comparison with
36 the widely applied PT-JPL model.

37 **1. Introduction**

38 Soil evaporation plays an important role in the mass and energy exchange between the
39 land surface and the atmosphere. Together with plant transpiration, they return about
40 60% of precipitation into the air (Oki & Kanae, 2006) and consume nearly 25% of the
41 incoming solar radiation globally (Trenberth et al., 2009). Estimating soil evaporation
42 accurately and separating its contribution from the plant transpiration are crucial to
43 understand the water and energy cycles (Seneviratne et al., 2010; Wang & Dickinson,
44 2012; Maxwell & Condon, 2016; Gu et al., 2018) and to quantify the carbon cycle
45 process that is highly related to plant behavior (Sutanto et al., 2012; Schlesinger &
46 Jasechko, 2014; Fisher et al., 2017). Physically, soil evaporation is the transition of
47 soil water from the liquid phase to the vapor phase and the escape of water vapor to
48 the above atmosphere. The phase transition requires an energy supply while the vapor
49 escape is mainly a molecule diffusion process (Haghighi et al., 2013). By focusing
50 mainly on energy supply or on vapor transport process, the existing evaporation
51 estimation methods can generally be summarized into two series, the energy budget
52 one and the mass transfer one (Brutsaert, 2005).

53 The energy budget methods vary in different forms, among them, the classic one
54 relies on the concepts of atmospheric demand and water supply. The atmospheric

55 demand is represented by the potential evaporation rate, often estimated by the
56 Penman (1948) equation or by the Priestley & Taylor (1972) equation. The water
57 supply, also known as the water stress factor, is usually expressed empirically as a
58 linear function of soil water content after the identification of a “critical water content”
59 below which soil water supply is limited (Seneviratne et al., 2010). This kind of
60 method, also termed as the Bucket model (Budyko, 1974; Brutsaert, 2005), is
61 probably the oldest method of evaporation estimation. Due to its simplicity (which
62 may vary in different forms), it is still extensively applied, in particular within remote
63 sensing-based evaporation models (e.g., Fisher et al., 2008; Miralles et al., 2011;
64 Martens et al., 2017).

65 The mass transfer- or resistance-based methods consider the vapor transfer process in
66 a direct way. The evaporation process is described as vapor diffusion from either the
67 soil surface or a depth below. The former is the so-called α formulation (e.g., Barton,
68 1979; Noilhan & Planton, 1989). An aerodynamic resistance term is introduced to
69 represent the vapor transfer efficiency from soil surface to the atmosphere. When the
70 evaporation process is considered from a plane below the soil surface, where vapor
71 pressure is saturated, an additional soil surface resistance term is included, leading to
72 the so-called β formulation (e.g., Deardorff, 1977; Dorman & Sellers, 1989).

73 The Bucket model and the resistance-based methods, although widely applied, are
74 somehow empirically based, especially in determining the water stress and the
75 resistance factors. The linear relationship in the Bucket model is empirical (Brutsaert,
76 2005; Seneviratne et al., 2010) and might not be unique even in the same location
77 (Haghighi et al., 2018). The resistance methods, although physically based, rely on
78 empirical estimation of the resistance terms (e.g., Mahfouf & Noilhan, 1991; Merlin
79 et al., 2016, 2018). The ambiguities in parameter estimation methods, as well as the
80 difficulty in accurate data acquisition (e.g., the surface water content and the soil
81 hydraulic properties), therefore, would introduce high uncertainty in evaporation rate
82 estimation.

83 Alternatively, the soil evaporation can be estimated from the perspective of soil water
84 transport ability. Instead of being represented as a stress factor or a resistance term

85 (usually expressed empirically) as in the former methods, the soil water supply can be
86 calculated directly and the actual evaporation rate is regarded as the minimum term
87 between the soil water flux and the potential evaporation rate. This method is termed
88 as the threshold formulation (e.g., Mahrt & Pan, 1984; Dickinson, 1984). With the soil
89 water flux described physically by the Buckingham-Darcy's law, which can be
90 calculated by solving the Richards equation (e.g., Sutanto et al., 2012) or by
91 parameterizing over a thin soil surface layer (e.g., Mahrt & Pan, 1984), this method
92 provides a much more solid basis for evaporation estimation. In the literature, for a
93 drying process, capillary flow is regarded as the main soil water flow form and vapor
94 diffusion is included when soil becomes very dry (Philip & de Vries, 1957; Saito et al.,
95 2006; Lehmann et al., 2008; Or et al., 2013; Or & Lehmann, 2019).

96 However, such capillary flow- and vapor diffusion-supported evaporation process
97 may be problematic for not considering the potential impact of film flow. This thin
98 film form water, held by the adsorption forces on the soil particle surface, is usually
99 treated as unremovable and hence be unimportant in water flow process (e.g., Philip
100 & de Vries, 1957; Idso et al., 1974). Recent progress in soil hydraulic properties
101 modeling however has found that this film flow, is in fact the predominant water flow
102 form under low moisture conditions (e.g., Tuller & Or, 2001; Wang et al., 2013, 2018).
103 By including this film flow, the newly proposed soil hydraulic models greatly
104 improved the performance under low moisture conditions in comparison with
105 capillary-based models (Tuller & Or, 2001; Lebeau & Konrad, 2010; Peters, 2013;
106 Wang et al., 2016, 2017, 2018). The re-recognition of the importance of this thin
107 film, therefore, requires us to reconsider the soil evaporation process, which is
108 commonly assumed to be supported only by capillary flow and vapor diffusion.
109 Although early research in the engineering area has taken into account of the impact
110 of the so-called bound water (e.g., Chen & Pei, 1989), the analysis was problematic
111 due to the unclear definition of the hydraulic conductivity properties in relation to the
112 bound water.

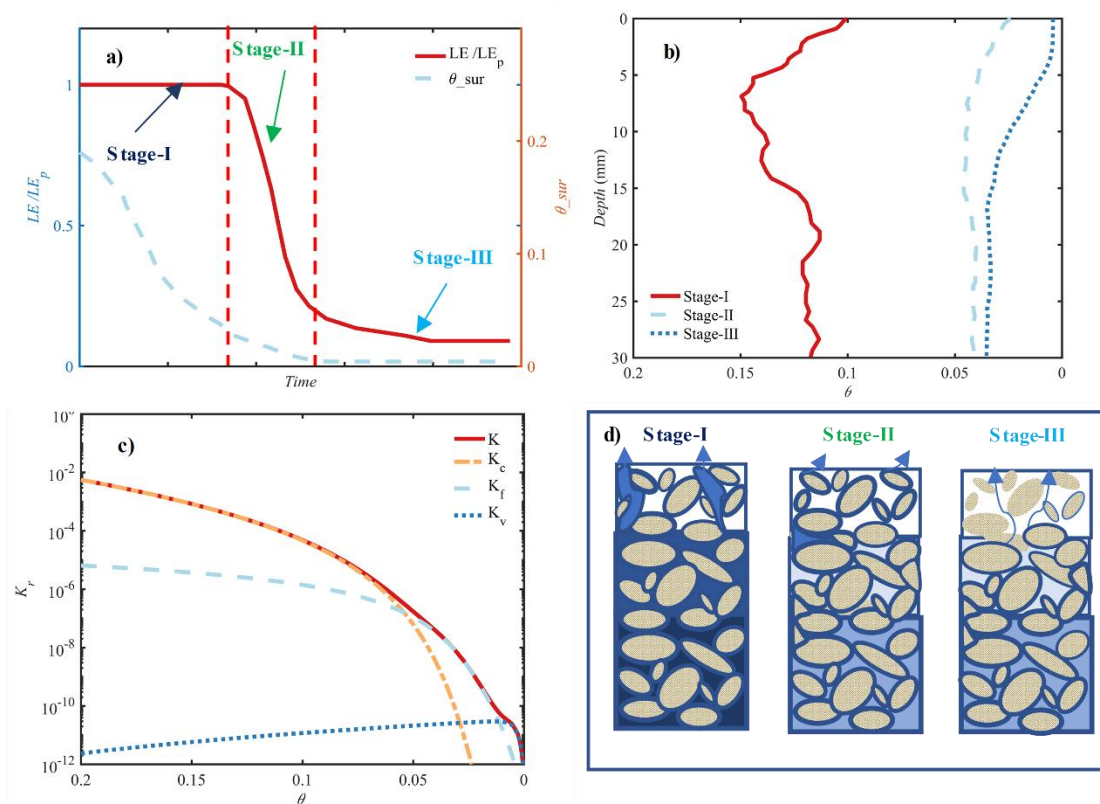
113 Hence, there are three main objectives in this study: 1) to reexamine the typical
114 evaporation process by including the impact of film flow, besides the commonly

115 recognized capillary flow and vapor diffusion; 2) to develop a theoretical evaporation
 116 estimation model based on the detailed analysis of the soil drying process; and 3) to
 117 evaluate the model performance with both laboratory and field observations.

118 2. Theoretical Development

119 2.1. The Soil Drying Process Revisited

120 [Figure 1 near here]



121

122

123 As shown in Figure 1 (a), the typical evaporation process from an initially saturated
 124 soil column can be generally distinguished into the energy-limited stage and the
 125 moisture-limited stage, respectively (e.g., Lehmann et al., 2008; Shokri et al., 2011;
 126 Or et al., 2013). The energy-limited stage is also termed as stage- I evaporation.
 127 When the atmospheric demand keeps constant, this stage would have a constant
 128 evaporation rate (assuming the impact of capillary limitations and nonlinear boundary
 129 layer interactions are not important), so it is also known as the constant-rate period
 130 (e.g., Yiotis et al., 2007). The moisture-limited stage can be subdivided into two

131 stages: the stage-**II** or the transition stage marked by a fast falling evaporation rate
132 and the stage-**III** where evaporation rate keeps low and changes smoothly (e.g., Idso et
133 al., 1974; Merz et al., 2015).

134 Correspondingly, the soil water flow supporting the drying process can also be
135 divided into three forms, including the commonly recognized capillary flow in full
136 pores and in corners and the vapor diffusion in void pores, as well as the usually
137 neglected thin film flow on soil particle surfaces (Tuller & Or, 2001; Peters, 2013;
138 Wang et al., 2018). Notably, this thin film flow held by adsorption forces is different
139 from the so-called “thick film flow” presented in the literature (e.g., Yiotis et al., 2003,
140 2007, 2012; Lehmann et al., 2008), where it represents the water flow supported
141 mostly by capillarity and controls the water transport between the saturated zone and
142 the evaporation surface. In these referred work, this thin film flow was assumed to be
143 unimportant and then be neglected (Yiotis et al., 2007).

144 **2.1.1. The Stage- I Evaporation**

145 For the drying process, the stage- I evaporation is extensively studied (e.g., Lehmann
146 et al., 2008, 2018; Shahraeeni et al., 2012; Shokri et al., 2008; Or et al., 2013 and
147 references therein). In this period, an efficient water supply between the drying front
148 and the soil surface is maintained by capillary flow. The drying process is
149 accompanied by a decrease in soil surface moisture and an increase in drying front
150 depth. The end of this period should depend on both the capillary flow ability and the
151 atmospheric demand. However, because the capillarity-supported water supply is
152 usually higher than the atmospheric demand even under low water saturation
153 conditions (Shahraeeni et al., 2012), the stage- I evaporation generally ends when a
154 critical surface water content or a characteristic depth is reached, where the capillary
155 water potential gradient between the drying front and the soil surface cannot
156 overcome the gravitational forces and viscous dissipation (Lehmann et al., 2008). This
157 critical water content then can be seen as air begins to invade the finest pores at soil
158 surface and it is roughly corresponding to the so-called residual water content (Or et
159 al., 2013). The duration of the stage- I evaporation is therefore determined by soil
160 pore size distribution properties. In this period, the evaporation rate is generally equal

161 to the potential evaporation rate. However, it should be noted that for very fine
162 textured soil and for high atmospheric demand, a higher critical water content and a
163 lower evaporation rate are expected due to the resistance induced by viscous effects
164 (Haghighi et al., 2013; Lehmann et al., 2018; Or & Lehmann, 2019) and/or due to the
165 vapor exchange limitations across the air boundary layer (Shahraeeni et al., 2012;
166 Haghighi & Or, 2013). In the present study, these effects are not included.

167 **2.1.2. The Stage- II Evaporation**

168 While extensive research on stage- I evaporation exists in the literature, little work
169 has been done on the stage- II evaporation (Shokri et al., 2011). In the classic soil
170 evaporation theory, when the capillary flow is interrupted at the end of stage- I
171 evaporation, the vaporization plane begins to recede into the inside soil and the vapor
172 diffusion becomes dominant at the soil surface (Philip & de Vries, 1957; Saito et
173 al., 2006; Lehmann et al., 2008; Or et al., 2013). Notably at this point, liquid water
174 still exists at soil surface, mainly in the form of thin film adsorbed by soil particle
175 (Tuller & Or, 2011; Wang et al., 2018). In the capillarity-based theory (e.g., van
176 Genuchten, 1980; Corey & Brooks, 1999), this left liquid water is represented by the
177 so-called residual water content and means the low limitation of the free soil water.
178 Accordingly, it has nearly no contribution to the evaporation process.

179 This left and unremovable soil surface water content, however, is inconsistent with
180 recent laboratory observations. . . For example, the magnetic resonance imaging of a
181 sand column presented by Merz et al. (2015) demonstrated clearly a gradual
182 decreasing soil surface moisture during the stage- II evaporation (see also Figure 1 b).
183 The vapor-diffusion-dominated assumption is also inconsistent with laboratory
184 observations. According to the Fick's law, a vapor-diffusion-controlled stage- II
185 evaporation requires a gradually increased diffusion layer thickness to explain the fast
186 falling evaporation rate (Shokri et al., 2009, 2011). The dye experiment by Shokri et
187 al. (2011) however observed an abrupt jump of the vaporization plane at the end of
188 the stage- II evaporation (the so-called transition period in Shokri et al., 2011). This
189 abrupt jump indicated that the vaporization plane should remain in the soil surface
190 during the stage- II evaporation. In other words, the water transport near the soil

191 surface is still dominated by liquid flow otherwise a gradually receding vaporization
192 plane would be observed. The gradually decreased soil surface moisture and the
193 dominant liquid flow observed in stage- II evaporation happens to be consistent with
194 recent progress in soil hydraulic properties modeling. Commonly used soil hydraulic
195 models conceptualize pore space as a bundle of cylindrical capillaries (e.g., van
196 Genuchten, 1980; Mualem, 1976), neglecting the flow in liquid films held by
197 adsorption forces. This kind of capillary models often underestimate the hydraulic
198 conductivities under dry conditions (e.g., Tuller & Or, 2001; Wang et al., 2013, 2018).
199 Recently, a lot of research confirms that the liquid film, also explained as in
200 corresponding to the residual water content in capillary model (Corey & Brooks,
201 1999), is actually flowable (Tuller & Or, 2001; Tokunaga, 2009; Wang et al., 2013;
202 Peters, 2013). By including both capillary flow and film flow, recently proposed
203 models significantly improve the model performance under dry conditions (Lebeau &
204 Konrad, 2010; Peters, 2013; Tuller & Or, 2001; Tuller et al., 1999; Wang et al., 2016,
205 2017, 2018). An illustration in Figure 1 (c) shows clearly that this neglected film
206 conductivity is dominating after the soil moisture reaches the so-called residual water
207 content while the vapor diffusion is only important under extremely dry conditions.

208 At pore scale, when air invades the finest pore at soil surface -marking the end of
209 stage- I evaporation-, liquid flow still exists in film form held by the adsorption force
210 as well as in corner form retained by capillarity. This is consistent with the following
211 statement made by Scherer (1990) for the fast falling rate evaporation period: “*The*
212 *liquid in the pores near the surface remains in the funicular condition, so there are*
213 *contiguous pathways along which flow can occur*” (see Figure 4 in Scherer, 1990).
214 Tuller & Or (2001) showed that the hydraulic conductivity resulting from corner flow
215 was generally negligible in comparison with film flow under dry conditions.
216 Therefore, the usually neglected film flow, rather than vapor diffusion, might be the
217 supporting mechanism that limits the water supply during stage- II evaporation. The
218 vapor diffusion also contributes to the evaporation process, however, in a magnitude
219 generally less than liquid film flow.

220 Notably this film dominant zone is restricted in a depth of several millimeters, below

221 which water flow is still supported by capillarity. During this stage, the evaporation
222 process is also accompanied by a decrease in soil surface moisture while the drying
223 front depth keeps almost constant due to the discontinuity of capillary flow (Lehmann
224 et al., 2008;). Because the film flow flux is controlled by the soil specific surface area
225 and the film thickness that depends on matric potential (Bird, 1960; Tokunaga, 2009),
226 when considering film flow limitations solely, the soils with finer texture should
227 generally have a higher evaporation rate (at the same matric potential) and a longer
228 decreasing period during stage- II evaporation.

229 **2.1.3. The Stage- III Evaporation**

230 The stage- III evaporation is therefore the period when vapor diffusion actually
231 controls (Shokri et al., 2011). As shown in Figure 1 (c), the vapor conductivity only
232 exceeds the film conductivity when soil water content is extremely low. In this stage,
233 the thin soil surface layer is (almost) completely dried (Figure 1 a and 1 b), with some
234 tightly-bounded thin liquid films left. The soil surface water content is equal to the
235 air-dry value. The evaporation process is accompanied by the receding of vaporization
236 plane (also known as the secondary drying front) into deeper soil. The vapor
237 diffusion-controlled evaporation rate is very low (Figure 1 a) and depends on the
238 diffusion length between vaporization plane and soil surface (Shokri et al., 2011).

239 **2.1.4. The Complete Evaporation Process**

240 By including film flow, the evaporation process can then be summarized into three
241 typical stages as shown in Figure 1 (d), with however some different explanations
242 with the classic theory: (1) The stage- I evaporation is supported by capillary flow
243 from drying front to soil surface. This stage ends when the driving capillary water
244 potential difference between drying front and soil surface cannot overcome the
245 gravitational forces and viscous dissipation, marked by a critical surface water content
246 or a characteristic drying depth (Lehmann et al., 2008). The duration of this stage
247 depends on the width of pore size distribution and is also impacted by the nonlinear
248 boundary layer interactions (Shahraeeni et al., 2012; Haghghi & Or, 2013) as well as
249 the soil texture-dependent capillary flow limitations (Haghghi et al., 2013; Lehmann
250 et al., 2018). When neglecting capillary flow limitations, the evaporation rate is

251 mainly controlled by the atmospheric demand. (2) The stage- II evaporation is also
252 supported by liquid flow, however, in the form of liquid film within a very thin soil
253 surface layer. The capillarity-driven water can no longer achieve the soil surface
254 directly. This stage ends when vapor conductivity becomes dominant over film
255 conductivity, marked with the jump of vaporization plane from surface to deeper soil.
256 The duration of this stage depends mainly on the specific surface area of porous
257 media. The evaporation rate is limited by the soil water transport ability mainly in
258 film form. (3) The stage- III evaporation is the vapor diffusion stage. An almost
259 completely dried layer is developed at the soil surface and it grows deeper and deeper
260 when the drying process keeps going. The evaporation rate depends on the depth of
261 the vaporization plane, which is also known as the secondary drying front.

262 At pore scale (Figure 1 d), the end of stage- I evaporation occurs when the air begins
263 to invade the finest pores at the soil surface. During the stage- II evaporation, almost
264 no saturated pores exist at the soil surface, liquid water is mainly retained in the form
265 of film and can move along the surface of porous media. In the stage- III evaporation,
266 almost no liquid water exists in pores and on the soil particle surface, except some
267 extremely thin films tightly bounded by adsorption force (depends on the air
268 humidity).

269 **2.2. Model Development**

270 **2.2.1. Accounting for Film Flow in the Evaporation Estimation**

271 Under most field atmospheric conditions, the evaporation rate is approximately equal
272 to potential evaporation during stage- I period. In stage- III period, the evaporation rate
273 is very low. Therefore, the key is to define the evaporation rate in stage- II evaporation.
274 because,

275 During stage- II period, the evaporation rate is limited by the soil water transport
276 ability, which can be expressed by the Buckingham-Darcy's law, written as

$$277 \quad LE = -K(\theta) \left. \frac{dh}{d\theta} \frac{d\theta}{dz} \right|_{z=0} \quad (1)$$

278 where LE ($L T^{-1}$) is the actual evaporation rate, and K ($L T^{-1}$) and h (L) are the
279 hydraulic conductivity and water potential at the surface water content θ , respectively.

280 When ignoring capillary flow limitations and nonlinear boundary layer interactions,
 281 the evaporation rate in stage- I period is equal to the potential evaporation rate, LE_p .
 282 Therefore, at the onset of stage- II evaporation, Eq. (1) becomes

$$283 \quad LE_c = -K(\theta_c) \left. \frac{dh}{d\theta} \frac{d\theta}{dz} \right|_{z=0, \theta=\theta_c} = LE_p \quad (2)$$

284 with θ_c being the critical surface water content marking the discontinuity of capillary
 285 flow. It is roughly close to the so-called residual water content (Lehmann et al., 2008;
 286 Or et al., 2013). It should be noted that when capillary flow limitations in relation to
 287 fine-textured soils (Haghighi et al., 2013) and/or vapor diffusion through above thin
 288 boundary layer in relation to high atmospheric demand (Shahraeeni et al., 2012)
 289 become be important in stage- I period, no constant evaporation rate stage would be
 290 observed and the LE_c might have a value less than LE_p (Lehmann et al., 2018; Or &
 291 Lehmann, 2019).

292 To solve Eqs. (1) and (2), information on the soil hydraulic properties are required. In
 293 the literature, the capillary based models, the van Genuchten (1980)-Mualem (1976)
 294 model for instance, are applied (e.g., Saito et al., 2006). This is questionable since the
 295 film flow, as discussed previously, is thought to be dominant during stage-II
 296 evaporation. According to Campbell & Shiozawa (1992), a linear relationship exists
 297 between water content and log-scale water potential under dry conditions, so that the
 298 soil water retention curve that accounts for film flow can be expressed as (Wang et al.,
 299 2016)

$$300 \quad S_f = \frac{\theta}{\theta_c} = 1 - \frac{\ln(h/h_c)}{\ln(h_0/h_c)} \quad (3)$$

301 with S_f being the saturation degree that accounts for film water, and h_c and h_0 the
 302 water potential at θ_c and zero, respectively. As suggested by Schneider & Goss (2012),
 303 h_0 can be approximately set to 6.3×10^4 m for soils with different texture properties.

304 The hydraulic conductivity that accounts for film flow depends on the soil specific
 305 surface area SA and the film thickness f (Bird, 1960), in the form of

$$306 \quad \frac{K(\theta)}{K(\theta_c)} = \frac{SA \times f^3}{SA_c \times f_c^3} \quad (4)$$

307 In general, the specific surface area is kept as constant in film conductivity models
 308 (Tuller & Or, 2001; Lebeau & Konrad, 2010; Wang et al., 2017). However, this
 309 assumption is not appropriate when film thickness is thick than the width of parallel
 310 plates or when the water film does not cover the entire soil surface under extremely
 311 dry conditions. When considering the sole contribution of film flow, an effective
 312 surface area can be applied. It was expressed as the water content to film thickness
 313 ratio, that is, $SA = \theta / f$. Since the soil surface water content is very low under stage- II
 314 evaporation, only van der Waals forces were considered. The film thickness formula
 315 proposed in Iwamatsu & Horii (1996) was applied, written as

$$316 \quad \frac{f}{f_c} = \left(\frac{h}{h_c} \right)^{-1/3} \quad (5)$$

317 Substituting Eq. (5) and $SA = \theta / f$ into Eq. (4) gives

$$318 \quad K(\theta) = K(\theta_c) S_f \left(\frac{h}{h_c} \right)^{-2/3} \quad (6)$$

319 Notably the impact of modified viscosity on film conductivity under very thin film
 320 thickness conditions (Tuller & Or, 2001; Lebeau & Konrad, 2010) was not considered
 321 here.

322 The water content gradient $d\theta/dz$ at soil surface is also required in Eqs. (1) and (2).
 323 The stage- II evaporation can be seen as a secondary drying process of a very thin soil
 324 layer (with several millimeters in length, see Figure 1 b) with uniform initial water
 325 content θ_c . Similar to the classic evaporation process as described in Gardner (1959)
 326 and in Brutsaert (2014), the upper boundary can be set to a fixed water content, θ_m ,
 327 which is actually the soil air-dry value. The value depends on the soil texture
 328 properties and the environmental conditions. The lower boundary can be set at a fixed
 329 depth defined as z_d , with the water content assigned as the surface water content,
 330 varying from θ_c to θ_m . When the water potential profile in the thin soil surface layer
 331 shows high nonlinearity, the water content profile can be seen as linear under dry
 332 conditions (Figure 1 b). Therefore, this gradient $d\theta/dz$ is approximately equal to $(\theta -$
 333 $\theta_m)/z_d$.

334 Dividing Eq. (1) by Eq. (2) and with the substitution of $d\theta/dz \approx (\theta - \theta_m)/z_d$ and Eqs. (3)
 335 and (6), one obtains

$$336 \quad \frac{LE}{LE_p} = S_f \left(\frac{h}{h_c} \right)^{1/3} \frac{(S_f - S_m)}{(1 - S_m)} \quad (7)$$

337 Eq. (7) provides a theoretical formula for scaling evaporation rate under stage-II
 338 evaporation, with the assumption that film flow dominates the soil surface water flow
 339 process. The normalized evaporation rate ranges from 1 at the beginning of stage-II
 340 evaporation to 0 when the air-dry soil water content is reached at the end of stage-II
 341 evaporation. Note that the impact of vapor diffusion is not considered in Eq. (7). This
 342 film-flow-based evaporation rate estimation method is simply termed as the E_FILM
 343 model.

344 The E_FILM model requires the input of soil surface water potential h , which is
 345 highly sensitive to water content and depends on soil texture properties. Alternatively,
 346 h can be calculated from the well-known Kelvin equation under dry conditions,
 347 assuming a thermodynamic equilibrium between liquid and vapor phase. Therefore, h
 348 can be written as:

$$349 \quad h = \frac{RT}{Mg} \ln(RH) \quad (8)$$

350 where R is the universal gas constant ($8.314 \text{ J mol}^{-1}\text{K}^{-1}$), T (K) is the absolute
 351 temperature, M is the molecular weight of water ($0.018015 \text{ kg mol}^{-1}$), g is the
 352 gravitational acceleration (9.81 m s^{-2}) and RH is the in-equilibrium relative humidity
 353 at soil surface. An illustration in Figure 2 (a) g shows that the temperature effect on
 354 water potential estimation is not significant. With neglecting the temperature effect,
 355 Eq. (7), therefore, can be written in the form of RH , as

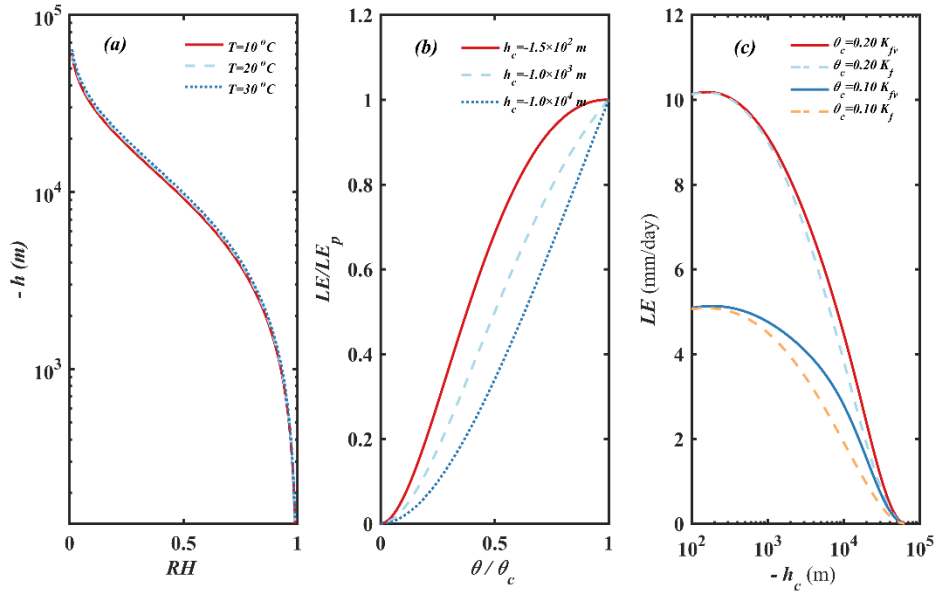
$$356 \quad \frac{LE}{LE_p} = \left[\frac{\ln(RH)}{\ln(RH_c)} \right]^{1/3} \frac{\ln[\ln(RH_0)/\ln(RH)]}{\ln[\ln(RH_0)/\ln(RH_c)]} \frac{\ln[\ln(RH_m)/\ln(RH)]}{\ln[\ln(RH_m)/\ln(RH_c)]} \quad (9)$$

357 where RH_0 is the in-equilibrium relative humidity at the water potential of h_0 , being
 358 1.04% at $20 \text{ }^\circ\text{C}$, while RH_c and RH_m are in corresponding to the water potential h_c and
 359 h_m , respectively.

360 The merit of using RH is that when vapor pressure is in equilibrium with soil water
361 potential, the RH keeps almost constant as 100% during stage- I evaporation since the
362 soil moisture supply is sufficient. It begins to decrease rapidly in stage- II evaporation
363 and then change slowly in stage-III evaporation, reflecting a moisture limited
364 condition. This changing is consistent with the evaporation rate dynamic. Hence, the
365 critical relative humidity RH_c and RH_m can be chosen as the maximum (except the
366 value of 1) and the minimum value of the observed RH , respectively. Tuller & Or
367 (2005) suggested an empirical threshold potential around -10^3 m (corresponding to a
368 RH of 93% at 20 °C) where the capillary condensation becomes negligible. When
369 continues observation of RH is unavailable, this empirical value is suggested as the
370 critical water potential value for different soils.

371 Eq. (9) provides a scaling method for soil evaporation estimation, requiring RH as the
372 sole input. As shown in Figure 2 (b), a nonlinear relationship exists between the
373 evaporation rate and the surface water content. It depends on the critical soil water
374 potential where stage- II evaporation begins. The more negative critical water
375 potential is expected for soils with finer texture under film flow limitations as
376 illustrated in Figure 2 (c). Notably here we didn't consider the possible impact of
377 capillary flow limitations. We emphasize here again that the E_FILM model deals
378 with the water flux in a very thin soil surface layer, with only several millimeters in
379 depth. Therefore, much negative matric potential values are expected compared to
380 those observed at much deeper layers in the literature.

381 **[Figure 2 near here]**



382

383 It is interesting to note that if the surface area SA was kept constant in Eq. (4), the
 384 E_FILM model would have the form of

385
$$\frac{LE}{LE_p} = \frac{S_f - S_m}{1 - S_m} \quad (10)$$

386 Eq. (10) yields a linear relationship between the scaled evaporation rate and the soil
 387 surface water content. It is in the same form as the widely applied but empirically
 388 based Bucket model (Budyko, 1974). Hence, Eq. (10) provides a physical explanation
 389 for the Bucket method. The slight difference between Eq. (10) and the Bucket model
 390 is that the soil water content in Eq. (10) is observed in a depth of several millimeters,
 391 while in the Bucket model, it generally represents a depth of several to tens of
 392 centimeters. However, the assumption that the water content shows a similar changing
 393 trend at different depths (near the soil surface) seems to be appropriate in the drying
 394 process.

395 The difference between Eqs. (7) and (10) comes from the different conductivity
 396 functions associated with film flow (Eq. 4). In deriving Eq. (7), only film-form water
 397 flow is considered, assuming no contribution comes from capillary flow when water
 398 content is less than the critical value θ_c . It represents a very dry condition under which
 399 the soil water potential dynamic can usually be captured by changes in RH (Tuller &
 400 Or, 2005). When stage- I evaporation ends at a more positive critical water potential

401 (in a magnitude cannot be captured by RH variation), water flow in the soil surface
402 might be supplied by both capillary flow (retained in very fine pores) and film flow
403 (along soil particle surface). Under this situation, Eq. (10) is preferred with the input
404 of soil surface water potential or water content. This is because the constant specific
405 surface area assumption in Eq. (4) generally yielded a close agreement with observed
406 conductivities in relatively high water potential range (Tuller & Or, 2001; Lebeau &
407 Konrad, 2010; Wang et al., 2017).

408 **2.2.2. The Impact of Capillary Flow Limitations in Stage- I Evaporation**

409 In the former section, it is assumed that the capillarity-driven water supply is
410 sufficient to meet the atmospheric water demand in stage- I, therefore, LE is equal to
411 LE_p for surface water content higher than θ_c (Eq. 2). However, when the capillary
412 flow limitations become be important in relation to fine-textured soils (Haghighi et al.,
413 2013; Lehmann et al., 2018; Or & Lehmann, 2019) and/or the vapor diffusion
414 limitations through the above thin boundary layer is significant under high
415 atmospheric demand (Shahraeeni et al., 2012), LE may also show a falling trend and
416 be less than LE_p during stage- I period.

417 Under this situation, the resistances come from capillary flow, film flow as well as
418 vapor diffusion should be taken into account together to describe a complete soil
419 evaporation process. Haghighi et al. (2013) and more recently, Lehmann et al. (2018)
420 provided a formula for describing the capillary limitations on evaporation rate. By
421 estimating LE_c in Eq. (2) with this formula, the evaporation rate dynamic during both
422 stage- I and stage- II period may be described. Such combination method, however,
423 requires a detail parameterization of soil hydraulic properties and involves a lot of
424 uncertainty. For example, due to the high specific surface area, the film flow may be
425 important even in stage-I period for fine textured soils. This possible impact however
426 was not taken into account in the existing theory that dealing with capillary
427 limitations (e.g., Haghighi et al., 2013; Lehmann et al., 2018). In the present study,
428 therefore, we focus solely on the limitations come from film flow in stage- II period
429 and ignore the possible impact of capillary flow limitations in stage- I period.

430 **2.2.3. The Impact of Vapor Flow**

431 Eq. (7) considers film flow only and ignores the potential impact of vapor transport
432 that is dominant during stage-III evaporation. Here, the isothermal vapor flow is
433 included to evaluate its influence on the evaporation rate. The vapor diffusion
434 contribution is calculated following the classical theory as provided in Philip & de
435 Vries (1957) and in Saito et al. (2006). The detail is presented in Appendix A. It
436 should be noted that only isothermal vapor diffusion is considered, so that the impact
437 of temperature gradient is not included.

438 Figure 2 (c) shows that the contribution of vapor flow is, in general, much less than
439 that of film flow. It is only important for soils with coarse texture and for very dry
440 conditions. Considering vapor flow in soil evaporation estimation, however, will
441 produce a very complex formula and requires additional information related to
442 specific soil properties. Here, we suggest a simple equation to include the impact of
443 vapor flow, written as:

$$444 \quad LE = S_f \left(\frac{h}{h_c} \right)^{1/3} \frac{(S_f - S_m)}{(1 - S_m)} (LE_p - LE_v) + LE_v \quad (11)$$

445 where LE_v represents the contribution from vapor flow. Shokri et al. (2011) showed
446 that the vapor diffusion flux was quite similar for soils with different texture, often in
447 a range from 0.5 to 2.5 mm d⁻¹ at the onset of stage-III evaporation. The mean vapor
448 diffusion rate is about 1.5 mm d⁻¹ for different soils. The accurate estimation of
449 vapor diffusion rate, however, requires the length between the vaporization plane and
450 the soil surface and requires also the atmospheric vapor pressure. Eq. (11) is only
451 suggested when vapor flow is believed to be important.

452 **2.2.4. Evaporation Rate Estimation in Field**

453 When it comes to field scale, the soil evaporation estimation becomes much more
454 complicated. In contrast with the monotonically increase of the film dominated soil
455 layer thickness as in laboratory experiment, the thin layer thickness under real field
456 conditions would grow and reduce during daytime and nighttime due to the soil
457 moisture redistribution (Brutsaert, 2014). As a result, a distinct diurnal pattern of
458 evaporation rate would be observed in field (e.g., Jackson et al, 1976; Idso et al., 1974,
459 1979). However, when considering the evaporation process at the daily scale, this

460 diurnal patter can be avoided (Brutsaert, 2014). The vapor transport can also be
461 neglected for its minor effect on the daily evaporation rate (e.g., Milly, 1984a, 1984b;
462 Saravanapavan & Salvucci, 2000).

463 Another difficulty with field data is that the relative humidity is often observed at the
464 height of 2 m above the soil surface, which might not be in equilibrium with soil
465 surface. However, the relative humidity at different heights generally shows a similar
466 trend during the evaporation process. Eq. (9) shows that it is the $\log(RH) / \log(RH_c)$
467 ratio that controls the value of LE . Therefore, it might be appropriate to assume that
468 the ratio of log-scale relative humidity at soil surface can be represented by that
469 observed at the height of 2 m. However, unlike laboratory experiments, it is hard to
470 define the critical RH_c where the evaporation rate begins to decrease as the
471 (atmospheric) boundary condition is an open system. In this study, a maximum value
472 of 0.85 derived by trial and error is suggested as the upper boundary for the critical
473 RH_c . That is, RH_c is the minimum value between 0.85 and the observed maximum RH .
474 RH_m is simply set to the minimum value of the observed RH . This requires the
475 observations cover a complete drying period. The influence of the soil heterogeneity
476 here is simplified by assuming that the applied air relative humidity represents a
477 mixture of soil surface moisture conditions.

478 With these assumptions and by ignoring vapor flow, Eq. (9) can now be used to
479 estimate the field soil evaporation rate, requiring only the meteorological data as input.
480 In this study, the potential evaporation rate LE_p is calculated by the Priestley & Taylor
481 (1972) equation, written as:

$$482 \quad LE_p = \alpha_{PT} \frac{\Delta}{\Delta + \gamma} (R_n - G) \quad (12)$$

483 where α_{PT} is the Priestley-Taylor constant, with the value of 1.26, Δ (kPa K⁻¹) the
484 slope of the vapor pressure curve at air temperature, γ (kPa K⁻¹) the psychrometric
485 constant, R_n (W m⁻²) the net radiation and G (W m⁻²) the soil heat flux.

486 **3. Data Description**

487 **3.1. Data from Laboratory Experiment**

488 The proposed E_FILM model is evaluated at both laboratory and field scales. The
489 laboratory data include nine thin (less than 1 mm in length) soil evaporation
490 experiments provided in Wilson (1990) and one thick soil column (50 cm in length)
491 evaporation experiment presented in Zhang et al. (2015).

492 **[Table 1 near here]**

493 The thin soil evaporation test includes three soil types, Beaver Creek Sand, Custom
494 Silt and Regina Clay. For each soil type, three tests were presented (see Table 1). In
495 all tests except for tests silt_1 and clay_1, the thin soil samples were prepared by
496 gently dusting a layer of dry soil onto a sheet of aluminum foil. The sample was then
497 saturated with distilled water using a mist applicator. For tests silt_1 and clay_1, the
498 soil sample was prepared as slurry and poured into the evaporation pan to achieve a
499 thicker soil layer. As described in Wilson (1990), some difficulties were encountered
500 when using the slurried soil method. For example, non-uniform drying was found for
501 silt_1 test and for clay_1 test. Besides, shrinking and deformation was frequently
502 observed for clay_1 test, which resulted in problems such as curling and irregular
503 drying. The evaporation was preceded in room temperature and the relative humidity
504 of air was kept almost constant. For the details please refer to Wilson (1990).

505 The thick soil evaporation experiment was provided in Zhang et al. (2015). The soil
506 column was 50 cm in length. Different from the thin soil evaporation, an infrared
507 lamp was used for supplying heat to soil surface. The relative humidity near soil
508 surface was recorded during the drying process. The experiment details can be seen in
509 Zhang et al. (2015).

510 **3.2. Data Collected from Field Sites**

511 The field sites are chosen from the collection presented in Merlin et al. (2016),
512 including 15 sites representing bare soil conditions across different countries (see
513 table 2). Note that only sites with more than 40 days of observation are selected.
514 These sites were selected mostly from the national and international flux station

515 networks (OZnet, European Flux Database and AmeriFlux) while two sites were
516 chosen from short term intensive field campaigns such as the HAPEX
517 (Hydrology-Atmosphere Pilot Experiment) and IHOP (International H2O Project).
518 Most of these sites, however, are not under true bare soil conditions. Merlin et al.
519 (2016) provided a principle for choosing the “bare soil” period where plant
520 transpiration is thought to be negligible. For more details please refer to Merlin et al.
521 (2016).

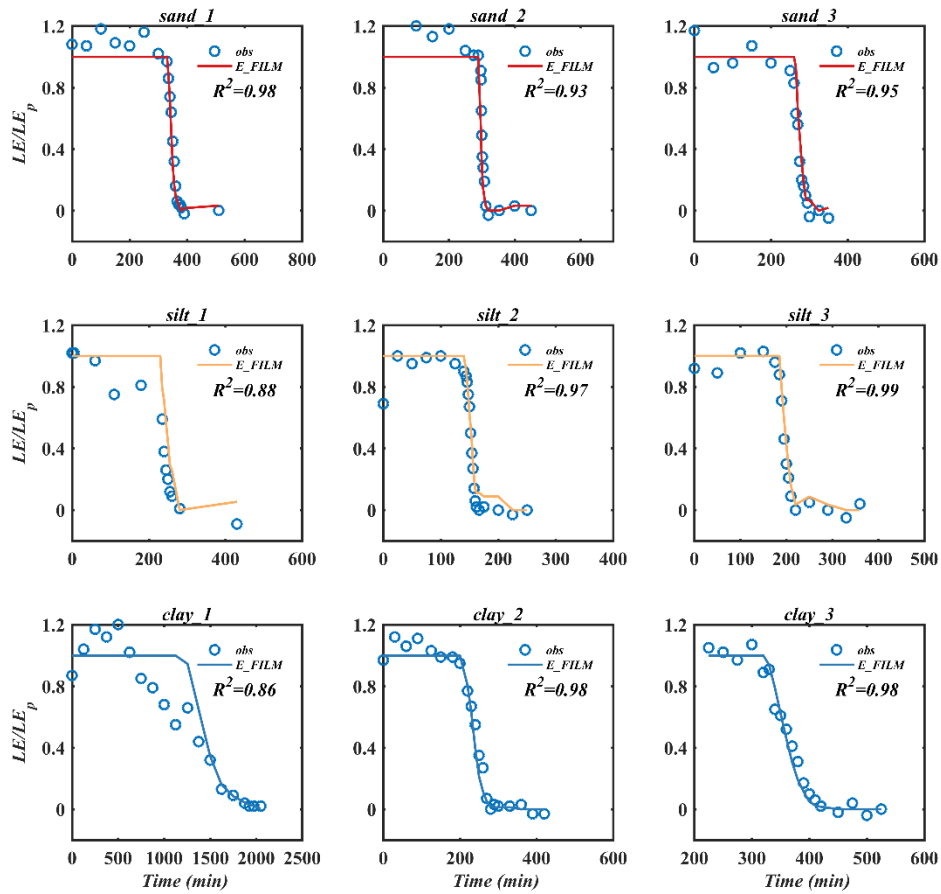
522 **[Table 2 near here]**

523 **4. Results and Discussion**

524 **4.1. Model Testing with Thin Soil Evaporation**

525 The thin soil evaporation presented in Wilson (1990) represents exactly the physical
526 process described by the E_FILM model, that is, a drying process of extremely thin
527 (less than 1 mm) soil layer. Hence there exists no impact of moisture supply from
528 below soil as in thick soil column evaporation. The vapor flow within soil can be
529 neglected because there is no moisture supply during stage-III evaporation. The soil
530 water potential was calculated from observed water content by the measured soil
531 water retention curve. The in-equilibrium relative humidity at soil surface is then
532 provided according to the Kelvin equation. Therefore, these thin soil evaporation
533 experiments provide the perfect data for model testing.

534 **[Figure 3 near here]**



535

536 Model testing results as shown in Figure 3 demonstrated clearly that the provided
 537 E_FILM model was in excellent agreement with observations for almost all nine
 538 experiments. Two exceptions are for tests silt_1 and clay_1, where the evaporation
 539 rate began to decrease while the observed RH kept constant as 1. As demonstrated in
 540 section 3.1, these two tests applied a different method for sample preparation and
 541 yielded a non-uniform drying process. This may explain the mismatch between model
 542 predictions and observations.

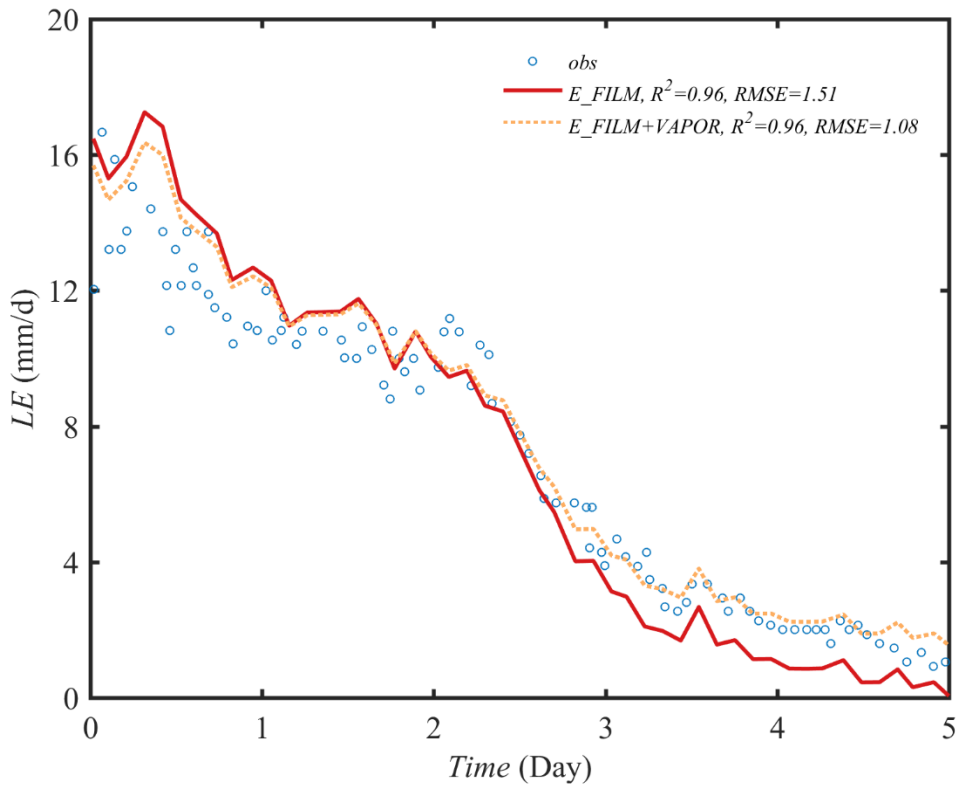
543 Another mismatch was observed during stage- I evaporation, where the observed soil
 544 evaporation was generally larger than the potential rate. In this experiment, the
 545 potential evaporation rate was observed from free water evaporation under the same
 546 environment. Therefore, this mismatch may be due to the different vapor diffusion
 547 through the thin atmospheric layer above soil and water surface, respectively. This
 548 issue is not in the scope of the E_FILM model.

549 When using E_FILM model to predict the evaporation rate, only in-equilibrium RH

550 and potential evaporation rate LE_p are needed, requiring no adjustable parameter in
551 relation to soil texture. The different evaporation rate change among different soils
552 have already been captured by the in-equilibrium RH . According to Figure 2 (c), the
553 critical matric potential is expected to be smaller (more negative) for soils with finer
554 texture under film flow limitations situation. On the contrary, the observed RH_c was
555 close to 0.99 (corresponding to a water potential of -138 m at 20°C) for all soils. This
556 may be explained by that the critical matric potential that marks the beginning of
557 stage- II evaporation is too large (higher than -138 m for all soils) to be captured by
558 RH observations. This is consistent with the description of the evaporation process in
559 section 2.1, where the critical water potential is thought to be close to the value in
560 corresponding to the residual water content. In the literature (e.g., Wang et al., 2016;
561 2017), this value was generally higher than -138 m, especially for soils with coarse
562 texture. Nevertheless, as soon as the soil water supply cannot meet the atmospheric
563 demand, the soil surface water potential would decrease dramatically to very negative
564 values, resulting in a decrease of observed RH .

565 **4.2. Model Testing with Soil Column Evaporation**

566 **[Figure 4 near here]**



567

568 The sand column evaporation experiment presented in Zhang et al. (2015) was
 569 undertaken with an external heat supply, resulting in much low RH observations near
 570 soil surface, changing from 18% to 58%. Therefore, the soil water potential may not
 571 be in equilibrium with the observed RH . However, as discussed previously, it is the h/h_c
 572 ratio that controls the change of evaporation rate and the observed RH can then be
 573 used for predicting the evaporation rate. Besides, with external heat supply, the
 574 atmospheric demand was very high through the drying process. A decreasing
 575 evaporation rate was observed during stage- I period (Figure 4). This might be
 576 attributed to the vapor diffusion limitations through above thin boundary layer
 577 (Shahraeni et al., 2012). This effect is not included in the E_FILM model
 578 development. Therefore, we only considered the drying process after stage- I period
 579 and the critical RH_c was chosen at day 2 from RH observations.

580 Figure 4 showed that the estimated evaporation rate was generally in good agreement
 581 with observations. An underestimation however was found in the low evaporation rate
 582 range. Different from the thin soil evaporation, the vapor flow can be important in the
 583 soil column evaporation case, especially during stage-III evaporation. By including

584 vapor flow and by setting LE_v to 1.5 mm d^{-1} (the mean vapor diffusion rate from
585 Shokri et al. 2011) in Eq. (11), the model estimation was in excellent agreement with
586 observations (after days 2).

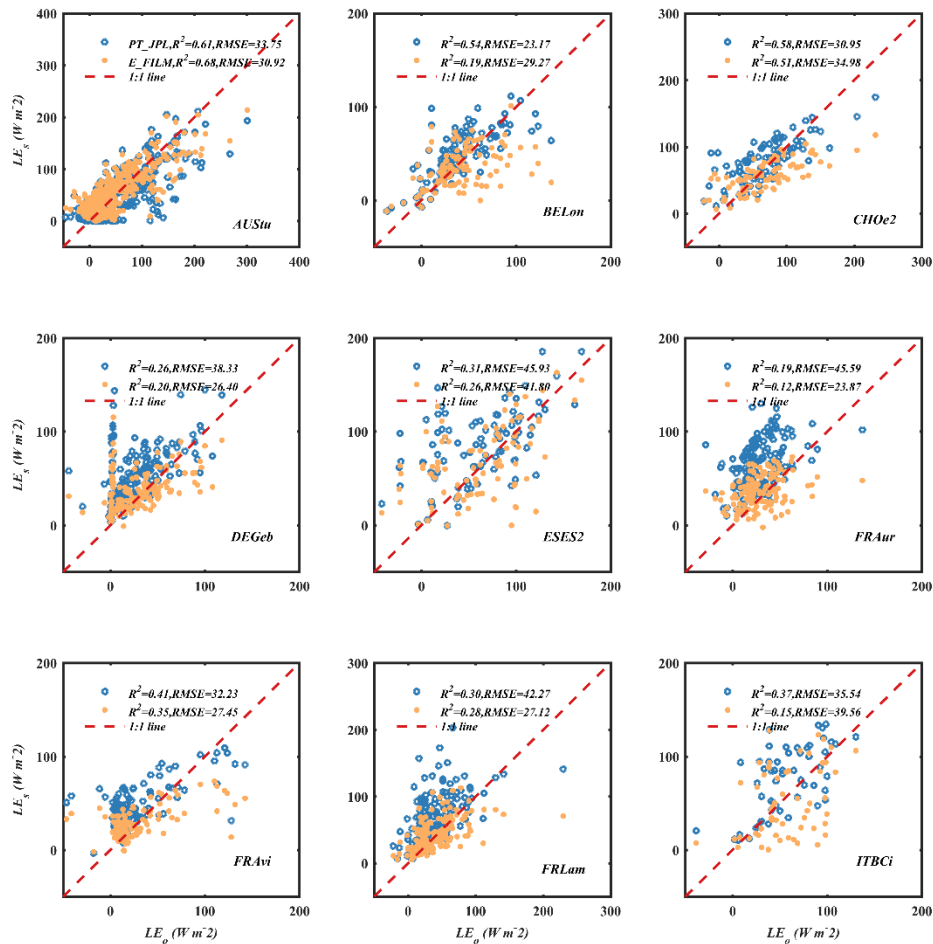
587 Here, no enhancement factor in relation to vapor diffusion is included (Shokri et al.
588 2011). The close agreement with observations when considering both film flow and
589 isothermal vapor diffusion might indicate that the unclearly defined enhancement
590 factor (e.g., Saito et al., 2006) actually represents the impact of film flow. However,
591 more testing with different soil columns are needed.

592 The excellent agreement with the observations of both thin soil and thick soil column
593 evaporation revealed that the E_FILM model (without adjustable parameter) might
594 have captured the actual physical mechanism during stage- II evaporation.

595 **4.3. Model Testing with Field Observations**

596 When testing the E_FILM model with field observations, significant uncertainties are
597 visible. The main reason is the lack of RH observations at the soil surface. When
598 using the RH observed at 2 m instead, it is difficult to define the critical RH_c as the
599 humidity is not only impacted by soil wetness but also by other atmospheric factors.
600 Under wet conditions, the RH at soil surface is generally higher than that at 2 m above,
601 and therefore, the critical RH_c when using observations at 2 m should have a value
602 smaller than that (close to 0.99) observed in laboratory. In this study, a maximum
603 value of 0.85 derived by trial and error is suggested as the upper boundary for the
604 critical RH_c . For model illustration, the soil evaporation module from the widely
605 applied PT-JPL model (Fisher et al., 2008) was chosen for comparison. This module
606 uses an empirical equation to express the water stress, also as a function of RH (see
607 Appendix B).

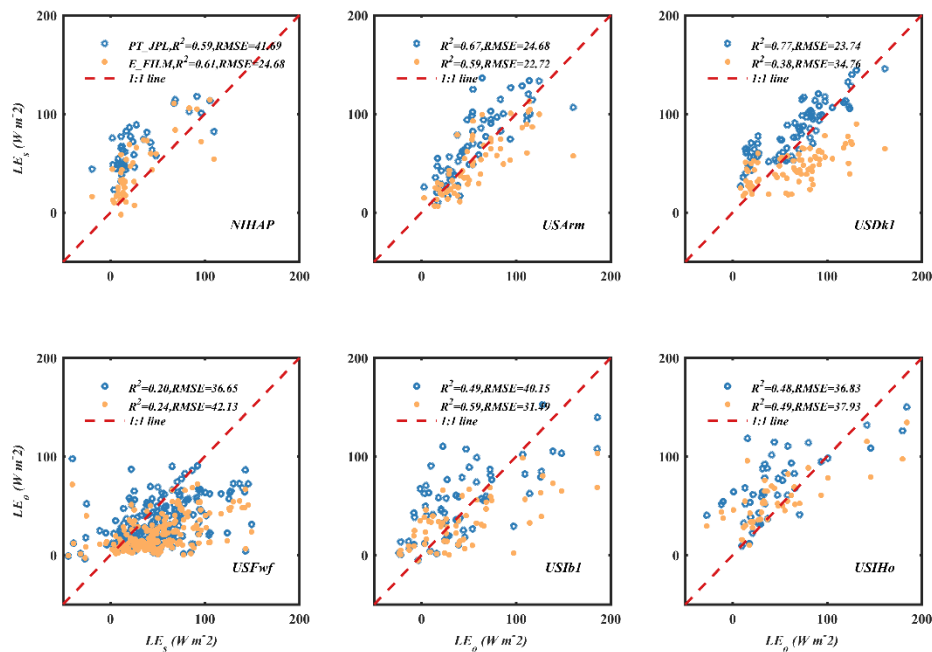
608 **[Figure 5 near here]**



609

610 Model testing with 15 sites as shown in Figures 5 and 6 demonstrated that the
 611 E_FILM model generally captured the dynamics of evaporation observations.
 612 Especially, the E_FILM model improved the prediction under low evaporation
 613 conditions in comparison with the PT-JPL model, as shown at sites DEGeb, FRAur,
 614 FRAvi, FRLam and NIHAP. The overestimation of evapotranspiration (ET) rates
 615 under arid and semi-arid sites was known to be a common problem in almost all ET
 616 models (e.g., Michel et al., 2016). Therefore, the developed E_FILM model may
 617 provide a possible solution for this problem.

618 **[Figure 6 near here]**



619

620 The E_FILM model underestimated evaporation rate at sites BELon, USDK1 and
 621 USFwf. This underestimation can be improved by choosing a lower RH_c , indicating
 622 that the critical value is actually different under different conditions.

623 In summarize, the E_FILM model generally yielded lower RMSEs in comparison
 624 with the PT-JPL model, with a mean value of $31.67 W m^{-2}$ and $35.43 W m^{-2}$,
 625 respectively (Figures 5 and 6). For R^2 , however, the PT-JPL model generally
 626 presented higher values, with a mean value of 0.45 compared to the 0.38 of the
 627 E_FILM model. This much lower R^2 with the E_FILM model was mainly due to the
 628 poor performance at sites BELon and USDK1.

629 The relatively poor performance with field observations might be due to two main
 630 reasons. Firstly, most testing sites were not in a true bare soil situation. As shown in
 631 table 2, only two sites (NIHAP and USIHO) were under bare soil condition while the
 632 observations from other sites were chosen from a “bare soil” period assuming plant
 633 transpiration was “negligible or small compared to soil evaporation” (Merlin et al.,
 634 2016). However, without direct measurement of the soil evaporation, it is hard to
 635 evaluate the data quality. Secondly, high uncertainty existed in relation to the RH
 636 input. In this study, the RH data used were observed at 2 m above the soil surface and
 637 should be different from the in-equilibrium RH at the soil surface. Besides, an upper

638 boundary of 0.85 was set for the critical RH_c in this study. However, as discussed
639 previously, this value might be different at different sites. For example, the
640 underestimation at sites BELon and USDK1 can be improved by setting a lower
641 critical RH_c . However, it was hard to define the actual RH_c since this value was not
642 only related to soil texture but also to atmospheric conditions. Uncertainty also
643 existed in defining RH_m . In this study, RH_m was simply set as the lowest value of the
644 observed RH . This principle was appropriate only when the observations covered a
645 complete drying period. Note that the impacts of RH_c and RH_m are highly correlated
646 in the E_FILM model.

647 In spite of this disadvantage, the E_FILM model was attractive for its solid physical
648 base, which was evidenced by laboratory observations. Moreover, the estimation of
649 soil evaporation in field showed an improvement under dry conditions. The film
650 dominant assumption in the E_FILM model was also consistent with the field drying
651 experiment in Goss & Madliger (2007), where they found the film flow has a
652 significant contribution in soil evaporation. However, further work is needed to
653 derive a complete evaporation rate estimation model by including both capillary and
654 film limitations, and to improve the model performance in field, for example,
655 considering the input of soil surface water content.

656 **5. Conclusions**

657 This study provided a new interpretation of the typical soil evaporation process by
658 including the impact of film flow along the soil particle surface. This film flow was
659 usually thought to be unimportant and then be neglected in soil drying process (e.g.,
660 Philip & de Vries, 1957; Idso et al., 1974). However, recent progress in soil hydraulic
661 modeling development confirmed this film flow as a dominant process under low
662 moisture conditions (e.g., Tuller & Or, 2001; Peters, 2013; Wang et al., 2016, 2017,
663 2018). By including this film flow, the typical drying process was revisited. The result
664 found that this film flow might be the dominant process for limiting the evaporation
665 loss under stage- II evaporation, in which the vapor flow was usually regarded as the

666 limitation factor (e.g., Philip & de Vries, 1957; Saito et al., 2006; Lehmann et al.,
667 2008; Or et al., 2013). The typical evaporation process was then interpreted as the
668 capillary-flow-supported stage- I evaporation, the film-flow-controlled stage- II
669 evaporation and the vapor-diffusion-dominant stage- III evaporation.

670 Based on the assumption that film flow controlled the stage- II evaporation, a
671 physically based model was developed by parameterizing the Buckingham-Darcy's
672 law. The model provided a solid basis for describing the moisture limitation on
673 evaporation rate, requiring only meteorological data as input and introducing no
674 adjustable parameter. The impact of vapor flow was also discussed. It was found to be
675 only important for soils with coarse texture under very dry conditions.

676 Model testing with laboratory data, including nine thin soil thickness evaporation tests
677 and one thick sand column evaporation, yielded excellent agreement with
678 observations. The model evaluation with 15 field sites however introduced some
679 uncertainty. The main reason is the lack of in-equilibrium relative humidity
680 observations near the soil surface. Nevertheless, the proposed E_FILM model
681 significantly improves the performance under dry conditions in comparison with the
682 widely applied PT-JPL model. Since the evaporation overestimation in arid and
683 semi-arid regions has been found in almost all evapotranspiration estimation models
684 (Michel et al., 2016), this E_FILM model provides an opportunity to improve the
685 evaporation estimation under such dry conditions. However, the present E_FILM
686 model didn't consider the impact of capillary limitations which might be important in
687 fine-textured soils (Haghighi et al., 2013; Lehmann et al., 2018) and further work is
688 needed to test and improve the model performance in field, especially in relation to
689 the determination of the critical RH_c that marks the beginning of stage- II evaporation.

690 **Appendix A**

691 When both film flow and vapor diffusion are included, the evaporation rate can be
692 expressed by parameterizing the Buckingham-Darcy's law (Eq. 7), as

693
$$LE \approx (K_f + K_v) h \ln \left(\frac{h_0}{h_c} \right) \frac{(S_f - S_m)}{z_d} \quad (\text{A1})$$

694 where K_f and K_v are the hydraulic conductivity that accounts for film flow and
695 isothermal vapor flow, respectively.

696 By applying the effective surface area, the film conductivity is expressed as

697
$$K_f = \frac{2\rho g \theta_f}{3\pi\eta} f^2 \quad (\text{A2})$$

698 where ρ is the water density ($9.98 \times 10^2 \text{ kg m}^{-3}$), g is the acceleration of gravity (9.81
699 m s^{-2}), η is fluid viscosity ($1.005 \times 10^{-3} \text{ Pa s}$ at 293 K) and the film thickness f is
700 expressed following Tuller & Or (2001), as

701
$$f = \sqrt[3]{\frac{-A_{svl}}{6\pi\rho gh}} \quad (\text{A3})$$

702 where A_{svl} is the Hamaker constant for solid-vapor interactions through the
703 intervening liquid and is set as $-6.0 \times 10^{-20} \text{ J}$ following Tuller & Or (2001).

704 The isothermal vapor conductivity is given in Saito et al. (2006), as

705
$$K_v = \frac{\rho_v}{\rho} D \frac{Mg}{RT} RH \quad (\text{A4})$$

706 where ρ_v (kg m^{-3}) is the saturated vapor density, D ($\text{m}^2 \text{ s}^{-1}$) is the vapor diffusivity,
707 written as

708
$$D = \tau \theta_a D_a \quad (\text{A5})$$

709 with θ_a being the air-filled porosity, τ the tortuosity factor calculated according to
710 Millington and Quirk (1961), as

711
$$\tau = \frac{\theta_a^{7/3}}{\theta_s^2} \quad (\text{A6})$$

712 with θ_s the saturated water content.

713 And D_a is the vapor diffusivity in air, written as

714
$$D_a = 2.12 \times 10^{-5} \left(\frac{T}{273.15} \right)^2 \quad (\text{A7})$$

715 **Appendix B**

716 The soil evaporation in the PT-JPL model (Fisher et al., 2008) is estimated by

717
$$LE = RH^{VPD/\beta} LE_p \quad (\text{B1})$$

718 with VPD (kPa) being vapor pressure deficit, β (1.0 kPa) representing the relative
719 sensitivity to VPD.

720 **Acknowledgments**

721 The research was supported by the National Natural Science Foundation of China
722 (Nos. 41601030) and the National Key Research and Development Program of China
723 (2017YFC0406105) and the Fundamental Research Funds for Central Universities,
724 China University of Geosciences (Wuhan) (No. CUG1323531877). The laboratory
725 data is collected from the doctoral thesis of Graham W. Wilson (University of Kansas)
726 and from the research of Chenming Zhang (University of Queensland), both are
727 greatly acknowledged. The original field bare-soil data set was prepared in the frame
728 of the MIXMOD-E project (ANR-13-JS06-0003). We acknowledge the following
729 sites of the European Flux Database (BELon, CHOe2, DEGeb, ESES2, FRAur,
730 FRAvi, FRLam, ITBCi), the following AmeriFlux sites (USArm, USDk1, USFwf),
731 the following OzFlux site (AUStu), and the following short term intensive field
732 campaigns (HAPEX-Sahel and IHOP) for their data records. Data is available on
733 repository (<https://doi.org/10.6084/m9.figshare.8898923>). Finally, the authors thank
734 the editor, the associate editor, and all anonymous reviewers for their very insightful
735 and constructive comments on this manuscript.

736 **References**

- 737 Alaoui, A., & Goetz, B. (2008). Dye tracer and infiltration experiments to investigate
738 macropore flow. *Geoderma*, 144(1-2), 279-286.
- 739 Barton, I. J. (1979). A parameterization of the evaporation from nonsaturated surfaces.
740 *Journal of Applied Meteorology*, 18(1), 43-47.
- 741 Beringer, J., Hacker, J., Hutley, L. B., Leuning, R., Arndt, S. K., Amiri, R., ... &
742 Hocking, D. (2011). SPECIAL—Savanna patterns of energy and carbon integrated
743 across the landscape. *Bulletin of the American Meteorological Society*, 92(11),
744 1467-1485.
- 745 Béziat, P., Ceschia, E., & Dedieu, G. (2009). Carbon balance of a three crop
746 succession over two cropland sites in South West France. *Agricultural and Forest*
747 *Meteorology*, 149(10), 1628-1645.
- 748 Bird, R. B., W. E. Stewart, and E. N. Lightfoot (1960), *Transport Phenomena*, John
749 Wiley, New York.
- 750 Brutsaert, W. (2005). *Hydrology: an introduction*. Cambridge University Press.
- 751 Brutsaert, W. (2014). Daily evaporation from drying soil: Universal parameterization
752 with similarity. *Water Resources Research*, 50(4), 3206-3215.
- 753 Budyko, M. I. (1974). *Climate and life*. New York, NY: Academic Press.
- 754 Campbell, G.S., Shiozawa, S., (1992). Prediction of hydraulic properties of soils using
755 particle-size distribution and bulk density data. In: van Genuchten, M.Th., Leij, F.J.,
756 Lund, L.J. (Eds.), *Proceedings of the International Workshop on Indirect Methods*

757 *for Estimating the Hydraulic Properties of Unsaturated Soil*. Univ. of California,
758 Riverside, CA, USA, pp. 317–328.

759 Chen, P., & Pei, D. C. T. (1989). A mathematical model of drying processes.
760 *International Journal of Heat and Mass Transfer*, 32(2), 297–310

761 Corey, A. T., & Brooks, R. H. (1999). The Brooks-Corey relationships. In M. T. van
762 Genuchten, F. J. Leij, & L. Wu (Eds.), *Proceedings of the International Workshop*
763 *on Characterization and Measurement of the Hydraulic Properties of Unsaturated*
764 *Porous Media* (pp. 13–18). Riverside, CA: University of California.

765 Deardorff, J. (1977). A parameterization of ground-surface moisture content for use in
766 atmospheric prediction models. *Journal of Applied Meteorology*, 16(11),
767 1182-1185.

768 Denef, K., Del Galdo, I., Venturi, A., & Cotrufo, M. F. (2013). Assessment of soil C
769 and N stocks and fractions across 11 European soils under varying land uses. *Open*
770 *Journal of Soil Science*, 3(07), 297.

771 Dickinson, R. E. (1984). Modeling evapotranspiration for three - dimensional global
772 climate models. *Climate processes and climate sensitivity*, 29, 58-72.

773 Dore, S., Montes- Helu, M., Hart, S. C., Hungate, B. A., Koch, G. W., Moon, J. B., ...
774 & Kolb, T. E. (2012). Recovery of ponderosa pine ecosystem carbon and water
775 fluxes from thinning and stand- replacing fire. *Global change biology*, 18(10),
776 3171-3185.

777 Dorman, J. L., & Sellers, P. J. (1989). A global climatology of albedo, roughness
778 length and stomatal resistance for atmospheric general circulation models as

779 represented by the Simple Biosphere Model (SiB). *Journal of Applied*
780 *Meteorology*, 28(9), 833-855.

781 Fischer, M. L., Billesbach, D. P., Berry, J. A., Riley, W. J., & Torn, M. S. (2007).
782 Spatiotemporal variations in growing season exchanges of CO₂, H₂O, and sensible
783 heat in agricultural fields of the Southern Great Plains. *Earth Interactions*, 11(17),
784 1-21.

785 Fisher, J. B., Tu, K. P., & Baldocchi, D. D. (2008). Global estimates of the
786 land-atmosphere water flux based on monthly AVHRR and ISLSCP-II data,
787 validated at 16 FLUXNET sites. *Remote Sensing of Environment*, 112(3), 901-919.

788 Fisher, J. B., Melton, F., Middleton, E., Hain, C., Anderson, M., Allen, R., ... & Kilic,
789 A. (2017). The future of evapotranspiration: Global requirements for ecosystem
790 functioning, carbon and climate feedbacks, agricultural management, and water
791 resources. *Water Resources Research*, 53(4), 2618-2626.

792 Gardner, W. R. (1959). Solutions of the Flow Equation for the Drying of Soils and
793 Other Porous Media 1. *Soil Science Society of America Journal*, 23(3), 183-187

794 Garrigues, S., Olioso, A., Calvet, J. C., Martin, E., Lafont, S., Moulin, S., ... &
795 Renard, D. (2014). Evaluation of land surface model simulations of
796 evapotranspiration over a 12 year crop succession: impact of the soil hydraulic
797 properties. *Hydrology and Earth System Sciences Discussions*, 11(10),
798 11687-11733.

799 Goss, K. U., & Madliger, M. (2007). Estimation of water transport based on in situ
800 measurements of relative humidity and temperature in a dry Tanzanian soil. *Water*
801 *resources research*, 43(5).

802 Gu, C., Ma, J., Zhu, G., Yang, H., Zhang, K., Wang, Y., & Gu, C. (2018). Partitioning
803 evapotranspiration using an optimized satellite-based ET model across biomes.
804 *Agricultural and forest meteorology*, 259, 355-363.

805 Haghghi, E., Shahraeeni, E., Lehmann, P., & Or, D. (2013). Evaporation rates across
806 a convective air boundary layer are dominated by diffusion. *Water Resources*
807 *Research*, 49(3), 1602-1610.

808 Haghghi, E., & Or, D. (2013). Evaporation from porous surfaces into turbulent
809 airflows: Coupling eddy characteristics with pore scale vapor diffusion. *Water*
810 *Resources Research*, 49(12), 8432-8442.

811 Haghghi, E., Short Gianotti, D. J., Akbar, R., Salvucci, G. D., & Entekhabi, D.
812 (2018). Soil and Atmospheric Controls on the Land Surface Energy Balance: A
813 Generalized Framework for Distinguishing Moisture - Limited and Energy -
814 Limited Evaporation Regimes. *Water Resources Research*, 54(3), 1831-1851.

815 Idso, S. B., Reginato, R. J., Jackson, R. D., Kimball, B. A., & Nakayama, F. S. (1974).
816 The Three Stages of Drying of a Field Soil 1. *Soil Science Society of America*
817 *Journal*, 38(5), 831-837.

818 Idso, S. B., Reginato, R. J., & Jackson, R. D. (1979). Calculation of evaporation
819 during the three stages of soil drying. *Water Resources Research*, 15(2), 487-488.

820 Iwamatsu, M., & Horii, K. (1996). Capillary condensation and adhesion of two wetter
821 surfaces. *Journal of colloid and interface science*, 182(2), 400-406.

822 Jackson, R. D., Idso, S. B., & Reginato, R. J. (1976). Calculation of evaporation rates
823 during the transition from energy- limiting to soil- limiting phases using albedo
824 data. *Water Resources Research*, 12(1), 23-26.

825 Kutsch, W. L., Aubinet, M., Buchmann, N., Smith, P., Osborne, B., Eugster, W., ... &
826 Ceschia, E. (2010). The net biome production of full crop rotations in
827 Europe. *Agriculture, ecosystems & environment*, 139(3), 336-345.

828 Lebeau, M., and J.-M. Konrad (2010), A new capillary and thin film flow model for
829 predicting the hydraulic conductivity of unsaturated porous media, *Water Resour.*
830 *Res.*, 46, W12554, doi:10.1029/2010WR009092.

831 Lehmann, P., Assouline, S., & Or, D. (2008). Characteristic lengths affecting
832 evaporative drying of porous media. *Physical Review E*, 77(5), 056309.

833 Lehmann, P., Merlin, O., Gentine, P., & Or, D. (2018). Soil Texture Effects on
834 Surface Resistance to Bare - Soil Evaporation. *Geophysical Research Letters*,
835 45(19), 10-398.

836 LeMone, M. A., Chen, F., Alfieri, J. G., Cuenca, R. H., Hagimoto, Y., Blanken, P., ...
837 & Grossman, R. L. (2007). NCAR/CU surface, soil, and vegetation observations
838 during the International H2O Project 2002 field campaign. *Bulletin of the American*
839 *Meteorological Society*, 88(1), 65-82.

840 Mahfouf, J. F., & Noilhan, J. (1991). Comparative study of various formulations of
841 evaporations from bare soil using in situ data. *Journal of Applied Meteorology*,
842 30(9), 1354-1365.

843 Mahrt, L., & Pan, H. (1984). A two-layer model of soil hydrology. *Boundary-Layer*
844 *Meteorology*, 29(1), 1-20.

845 Martens, B., Gonzalez Miralles, D., Lievens, H., Van Der Schalie, R., De Jeu, R. A.,
846 Fernández-Prieto, D., ... & Verhoest, N. (2017). GLEAM v3: Satellite-based land
847 evaporation and root-zone soil moisture. *Geoscientific Model Development*, 10(5),
848 1903-1925.

849 Maxwell, R. M., & Condon, L. E. (2016). Connections between groundwater flow and
850 transpiration partitioning. *Science*, 353(6297), 377-380.

851 Merlin, O., Stefan, V. G., Amazirh, A., Chanzy, A., Ceschia, E., Er- Raki, S., ... &
852 Beringer, J. (2016). Modeling soil evaporation efficiency in a range of soil and
853 atmospheric conditions using a meta- analysis approach. *Water Resources*
854 *Research*, 52(5), 3663-3684.

855 Merlin, O., Olivera-Guerra, L., Hssaine, B. A., Amazirh, A., Rafi, Z., Ezzahar, J., ...
856 & Er-Raki, S. (2018). A phenomenological model of soil evaporative efficiency
857 using surface soil moisture and temperature data. *Agricultural and Forest*
858 *Meteorology*, 256, 501-515.

859 Merz, S., Pohlmeier, A., Vanderborght, J., van Dusschoten, D., & Vereecken, H.
860 (2015). Transition of stage I to stage II evaporation regime in the topmost soil:

861 High-resolution NMR imaging, profiling and numerical simulation. *Microporous*
862 *and mesoporous materials*, 205, 3-6.

863 Michel, D., Jiménez, C., Miralles, D. G., Jung, M., Hirschi, M., Ershadi, A., ... &
864 Seneviratne, S. I. (2016). The WACMOS-ET project—Part 1: Tower-scale
865 evaluation of four remote-sensing-based evapotranspiration algorithms. *Hydrology*
866 *and Earth System Sciences*, 20(2), 803-822.

867 Millington, R. J., & Quirk, J. P. (1961). Permeability of porous solids. *Transactions of*
868 *the Faraday Society*, 57, 1200-1207.

869 Milly, P. C. D. (1984a). A linear analysis of thermal effects on evaporation from
870 soil. *Water Resources Research*, 20(8), 1075-1085.

871 Milly, P. C. D. (1984b). A simulation analysis of thermal effects on evaporation from
872 soil. *Water Resources Research*, 20(8), 1087-1098.

873 Miralles, D. G., Holmes, T. R. H., De Jeu, R. A. M., Gash, J. H., Meesters, A. G. C.
874 A., & Dolman, A. J. (2011). Global land-surface evaporation estimated from
875 satellite-based observations. *Hydrology and Earth System Sciences*, 15(2), 453.

876 Mualem, Y. (1976). A new model for predicting the hydraulic conductivity of
877 unsaturated porous media. *Water resources research*, 12(3), 513-522.

878 Nash, J. E., & Sutcliffe, J. V. (1970). River flow forecasting through conceptual
879 models part I—A discussion of principles. *Journal of hydrology*, 10(3), 282-290.

880 Noilhan, J., & Planton, S. (1989). A simple parameterization of land surface processes
881 for meteorological models. *Monthly weather review*, 117(3), 536-549.

882 Novick, K. A., Stoy, P. C., Katul, G. G., Ellsworth, D. S., Siqueira, M. B. S., Juang,
883 J., & Oren, R. (2004). Carbon dioxide and water vapor exchange in a warm
884 temperate grassland. *Oecologia*, *138*(2), 259-274.

885 Oki, T., & Kanae, S. (2006). Global hydrological cycles and world water resources.
886 *Science*, *313*(5790), 1068-1072.

887 Or, D., Lehmann, P., Shahraeeni, E., & Shokri, N. (2013). Advances in soil
888 evaporation physics—A review. *Vadose Zone Journal*, *12*(4).

889 Or, D., & Lehmann, P. (2019). Surface evaporative capacitance—how soil type and
890 rainfall characteristics affect global scale surface evaporation. *Water Resources*
891 *Research*.

892 Papale, D., Reichstein, M., Aubinet, M., Canfora, E., Bernhofer, C., Kutsch, W., ... &
893 Yakir, D. (2006). Towards a standardized processing of Net Ecosystem Exchange
894 measured with eddy covariance technique: algorithms and uncertainty
895 estimation. *Biogeosciences*, *3*(4), 571-583.

896 Penman, H. L. (1948). Natural evaporation from open water, bare soil and grass.
897 *Proc. R. Soc. Lond. A*, *193*(1032), 120-145.

898 Peters, A. (2013), Simple consistent models for water retention and hydraulic
899 conductivity in the complete moisture range, *Water Resour. Res.*, *49*, 6765–6780,
900 doi:10.1002/wrcr.20548.

901 Philip, J. R., & De Vries, D. A. (1957). Moisture movement in porous materials under
902 temperature gradients. *Eos, Transactions American Geophysical Union*, *38*(2),
903 222-232.

904 Priestley, C. H. B., & Taylor, R. J. (1972). On the assessment of surface heat flux and
905 evaporation using large-scale parameters. *Monthly weather review*, 100(2), 81-92.

906 Saito, H., Šimůnek, J., & Mohanty, B. P. (2006). Numerical analysis of coupled
907 water, vapor, and heat transport in the vadose zone. *Vadose Zone Journal*, 5(2),
908 784-800.

909 Saravanapavan, T., & Salvucci, G. D. (2000). Analysis of rate-limiting processes in
910 soil evaporation with implications for soil resistance models. *Advances in water*
911 *resources*, 23(5), 493-502.

912 Scherer, G. W. (1990). Theory of drying. *Journal of the American Ceramic Society*,
913 73(1), 3-14.

914 Schlesinger, W. H., & Jasechko, S. (2014). Transpiration in the global water cycle.
915 *Agricultural and Forest Meteorology*, 189, 115-117.

916

917 Schneider, M., and K.-U. Goss (2012), Prediction of the water sorption isotherm in air
918 dry soils, *Geoderma*, 170, 64 - 69, doi:10.1016/j.geoderma.2011.10.008.

919 Seneviratne, S. I., Corti, T., Davin, E. L., Hirschi, M., Jaeger, E. B., Lehner, I., ... &
920 Teuling, A. J. (2010). Investigating soil moisture–climate interactions in a changing
921 climate: A review. *Earth-Science Reviews*, 99(3-4), 125-161.

922 Shahraeeni, E., Lehmann, P., & Or, D. (2012). Coupling of evaporative fluxes from
923 drying porous surfaces with air boundary layer: Characteristics of evaporation from
924 discrete pores. *Water Resources Research*, 48(9).

925 Shokri, N., Lehmann, P., Vontobel, P., & Or, D. (2008). Drying front and water
926 content dynamics during evaporation from sand delineated by neutron radiography.
927 *Water Resources Research*, 44(6).

928 Shokri, N., Lehmann, P., & Or, D. (2009). Critical evaluation of enhancement factors
929 for vapor transport through unsaturated porous media. *Water resources research*,
930 45(10).

931 Shokri, N., & Or, D. (2011). What determines drying rates at the onset of diffusion
932 controlled stage - 2 evaporation from porous media?. *Water Resources Research*,
933 47(9).

934 Sutanto, S. J., Wenninger, J., Coenders-Gerrits, A. M. J., & Uhlenbrook, S. (2012).
935 Partitioning of evaporation into transpiration, soil evaporation and interception: a
936 comparison between isotope measurements and a HYDRUS-1D model. *Hydrology
937 and Earth System Sciences*, 16(8), 2605-2616.

938 Tokunaga, T. K. (2009), Hydraulic properties of adsorbed water films in unsaturated
939 porous media, *Water Resour. Res.*, 45, W06415, doi:10.1029/2009WR007734.

940 Trenberth, K. E., Fasullo, J. T., & Kiehl, J. (2009). Earth's global energy budget.
941 *Bulletin of the American Meteorological Society*, 90(3), 311-324.

942 Tuller, M., D. Or, and L. M. Dudley, (1999), Adsorption and capillary condensation
943 in porous media: Liquid retention and interfacial configurations in angular
944 pores, *Water Resources Research*, 35(7), 1949-1964.

945 Tuller, M., and D. Or (2001), Hydraulic conductivity of variably saturated porous
946 media: Film and corner flow in angular pore space, *Water Resour. Res.*, 37(5),
947 1257–1276, doi:10.1029/2000WR900328.

948 Tuller, M., and D. Or (2005), Water films and scaling of soil characteristic curves at
949 low water contents, *Water Resources Research*, 41(9).

950 van Genuchten, M. Th. (1980), A closed-form equation for predicting the hydraulic
951 conductivity of unsaturated soils, *Soil Sci. Soc. Am. J.*, 44, 892–898,
952 doi:10.2136/sssaj1980.03615995004400050002x.

953 Wallace, J. S., Allen, S. J., Gash, J. H. C., Holwill, C. J., & Lloyd, C. R. (1993).
954 Components of the energy and water balance at the HAPEX-Sahel southern
955 super-site. *IAHS PUBLICATION*, 365-365.

956 Wang, K., & Dickinson, R. E. (2012). A review of global terrestrial
957 evapotranspiration: Observation, modeling, climatology, and climatic variability.
958 *Reviews of Geophysics*, 50(2).

959 Wang, Y., Ma, J., Zhang, Y., Zhao, M., & Edmunds, W. M. (2013). A new theoretical
960 model accounting for film flow in unsaturated porous media. *Water Resources*
961 *Research*, 49(8), 5021-5028.

962 Wang, Y., Ma, J., & Guan, H. (2016). A mathematically continuous model for
963 describing the hydraulic properties of unsaturated porous media over the entire
964 range of matric suctions. *Journal of Hydrology*, 541, 873-888.

965 Wang, Y., Ma, J., Guan, H., & Zhu, G. (2017). Determination of the saturated film
966 conductivity to improve the EMFX model in describing the soil hydraulic
967 properties over the entire moisture range. *Journal of hydrology*, 549, 38-49.

968 Wang, Y., Jin, M., & Deng, Z. (2018). Alternative model for predicting soil hydraulic
969 conductivity over the complete moisture range. *Water Resources Research*, 54(9),
970 6860-6876.

971 Wilson, G. W. (1990). *Soil evaporative fluxes for geotechnical engineering*
972 *problems* (Doctoral dissertation, University of Saskatchewan).

973 Wu, C., Chen, J. M., Pumpanen, J., Cescatti, A., Marcolla, B., Blanken, P. D., ... &
974 Soegaard, H. (2012). An underestimated role of precipitation frequency in
975 regulating summer soil moisture. *Environmental Research Letters*, 7(2), 024011.

976 Yiotis, A. G., Boudouvis, A. G., Stubos, A. K., Tsimpanogiannis, I. N., & Yortsos, A.
977 Y. (2003). Effect of liquid films on the isothermal drying of porous media. *Physical*
978 *Review E*, 68(3), 037303.

979 Yiotis, A. G., Tsimpanogiannis, I. N., Stubos, A. K., & Yortsos, Y. C. (2007).
980 Coupling between external and internal mass transfer during drying of a porous
981 medium. *Water Resources Research*, 43(6).

982 Yiotis, A. G., Salin, D., Tajer, E. S., & Yortsos, Y. C. (2012). Drying in porous media
983 with gravity-stabilized fronts: Experimental results. *Physical Review E*, 86(2),
984 026310. Zhang, C., Li, L., & Lockington, D. (2015). A physically based surface
985 resistance model for evaporation from bare soils. *Water Resources Research*, 51(2),
986 1084-1111.

987 **Figure captions**

988 **Figure 1.** (a) Illustration of the normalized evaporation rate and the predicted soil
989 surface water content from an initial saturated soil column. Three stages are identified,
990 including the near constant rate stage- I evaporation, the fast falling rate stage- II
991 evaporation and the smoothly changing stage- III evaporation. (b) The near surface soil
992 water content profiles observed by magnetic resonance imaging at different
993 evaporation stages after Merz et al. (2015). (c) Illustration of the soil hydraulic
994 conductivity curve over the complete moisture range with the EMFX model proposed
995 in Wang et al. (2016, 2017), including capillary flow (K_c), film flow (K_f) and vapor
996 diffusion (K_v). The vapor diffusion is calculated following Saito et al. (2006). (d)
997 Illustration of the typical soil water flow process under three stages, the soil particle is
998 in yellow and the water is in blue. The stage- I evaporation is supported by capillary
999 flow retained in soil pores, the drying process is accompanied by an increase in the
1000 drying front depth; During stage- II evaporation, capillary flow can no longer reach
1001 soil surface directly, the drying process is limited by film flow along soil particle
1002 surface, dominated in a thin -several millimeters in depth- soil surface layer; Under
1003 stage- III evaporation, this thin soil surface layer is almost completely dried (with
1004 water content be equal to the air-dry water content), vapor diffusion becomes the
1005 dominant process in this layer.

1006 **Figure 2.** (a) The relationship between water potential and relative humidity under
1007 different temperatures. (b) Illustration of the E_FILM model with different critical
1008 water potential values; the surface water content is calculated with Eq. (3). (c)
1009 Illustration of the evaporation rate calculated with different critical water content
1010 values; the solid line accounts for both film flow and vapor diffusion while the dashed
1011 line accounts for film flow only (see Appendix A). The air-dry water content θ_m is set
1012 as zero and the depth of the thin layer z_d is set as 5 mm for illustration.

1013 **Figure 3.** E_FILM model testing with thin soil evaporation experiments from Wilson
1014 (1990), including sand, silt and clay.

1015 **Figure 4.** E_FILM model testing with thick sand column evaporation experiment
 1016 from Zhang et al. (2015)

1017 **Figure 5.** Predicted evaporation flux with the E_FILM model and the PT-JPL model
 1018 in the first nine field sites, LE_o and LE_s are the observed and the simulated
 1019 evaporation rate, respectively.

1020 **Figure 6.** Predicted evaporation flux with the E_FILM model and the PT-JPL model
 1021 in last six field sites, LE_o and LE_s are the observed and the simulated evaporation rate,
 1022 respectively.

1023

1024 **Table captions**

1025

1026 **Table 1.** The laboratory evaporation tests from Wilson (1990) and Zhang et al. (2015)

Test No.	Soil Type	Sample Thickness (mm)	RH of air	Reference
Sand_1	Beaver Creek Sand	0.7	0.53	Wilson (1990)
Sand_2		0.5	0.44	
Sand_3		0.5	0.58	
Silt_1	Custom Silt	0.5	0.21	Wilson (1990)
Silt_2		0.3	0.39	
Silt_3		0.3	0.62	
Clay_1	Regina Clay	0.7	0.39	Wilson (1990)
Clay_2		0.3	0.35	
Clay_3		0.2	0.50	
Soil column	Medium Sand	500	0.50	Zhang et al. (2015)

1027

1028 **Table 2.** Flux Sites including bare soil periods, modified from Merlin et al. (2016)

Site	Exp./Net.	Lat;lon	Land cover	Soil Texture	Reference
AUStu	OzFlux	-17.15;133.35	grass	Silt loam	Beringer et al. (2011)

BELon	GHGEurope	50.55;4.74	crop	Silt loam	Papale et al. (2006)
CHOe2	GHGEurope	47.29;7.73	crop	Silty clay	Alaoui and Goetz (2008)
DEGeb	GHGEurope	51.10;10.91	crop	Silty clay loam	Kutsch et al. (2010)
ESES2	GHGEurope	39.28; -0.32	crop	Silty clay	Kutsch et al. (2010)
FRAur	GHGEurope	43.55;1.11	crop	Clay loam	Béziat et al. (2009)
FRAvi	GHGEurope	43.92;4.88	crop	Silty clay loam	Garrigues et al. (2015)
FRLam	GHGEurope	43.50;1.24	crop	Clay	Béziat et al. (2009)
ITBCi	GHGEurope	40.52;14.96	crop	Clay	Denef et al. (2013)
NIHAP	HAPEX	2.24;13.20	bare	Sand	Wallace et al. (1993)
USArm	AmeriFlux	36.61; -97.49	crop	Clay	Fischer et al. (2007)
USDk1	AmeriFlux	35.97; -79.09	grass	Loam	Novick et al. (2004)
USFwf	AmeriFlux	35.45; -111.77	grass	Silt loam	Dore et al. (2012)
USIb1	AmeriFlux	41.86; -88.22	crop	Silty clay loam	Wu et al. (2012)
USIHO	IHOP	36.47; 100.62	bare	Sandy clay loam	Lemone et al. (2007)
